Physica Scripta

PAPER

Longitudinal one-dimensional mechanical topological insulator

Madeleine Hoag Carhart[*,1], **Parker Fairfield**[*,1], **Juan M Merlo**[*,1], **Luke Thatcher**[2] and **Lázaro Merlo-Ramírez**[3]

[1] Physics and Astronomy Department. Vassar College, 124 Raymond Ave. Poughkeepsie, NY, 12604, United States of America
[2] Department of Mechanical Engineering, University of New Hampshire, 33 Academic Way, Durham, NH, 03824, United States of America
[3] Instituto Tecnológico de Puebla, Av. del Tecnológico No. 420. Col. Maravillas. Puebla, Pue., 72220, Mexico
[*] These authors contributed equally to this work.

E-mail: jmerloramirez@vassar.edu

RECEIVED
24 July 2024

REVISED
1 October 2024

ACCEPTED FOR PUBLICATION
16 October 2024

PUBLISHED
28 October 2024

Keywords: topological insulators, mechanical, one-dimensional SSH

Supplementary material for this article is available online

Abstract

We present a study of a longitudinal one-dimensional mechanical topological insulator based on a slinky spring in the Su-Schrieffer-Heeger (SSH) configuration. The system demonstrates key characteristics of topological insulators, including the existence of edge states in the bandgap, exponential decay of amplitude, and a winding number of 1 for topological phases. By manipulating the stiffness of the spring through the placement of masses, we transition between trivial, metallic, and topological phases. Our findings also show that the edge states are robust against perturbations, and we observe a critical phase transition where the coherence length follows a critical exponent of -1, as predicted by theory. This simple mechanical system provides an accessible platform for studying the special properties of topological insulators and opens up new possibilities for exploring topological phenomena in classical systems.

1. Introduction

Topological insulators (TIs) are a distinct state of matter that has attracted considerable attention in the field of condensed matter physics for the last twenty years [1]. TIs differ from typical insulators in that they allow current conduction on their surface or edges—called surface or edge states—while still preserving insulating qualities in their interior [2–4]. This phenomenon occurs as a result of topological features in the material's electronic band structure, which are resistant to disturbances like impurities and defects [4]. The presence of time-reversal symmetry ensures the protection of these surface/edge states, resulting in notable characteristics such as spin-momentum locking and resistance to backscattering [1–4]. Although TIs were first found in quantum systems [3, 4], the foundations of topological insulators do not rely exclusively on quantum phenomena [5]. This led to the exploration of topological phases in classical systems, which have been observed with acoustic [6, 7], photonic [8, 9], and mechanical waves [10, 11].

Su, Schrieffer, and Heeger proposed a model to explain the existence of solitons in polyacetylene [12]. This model has been called the SSH model and has be an important reference for the study of topological phases in one-dimensional structures not only in quantum systems but also in classical applications [11, 13, 14]. There are three unique topologies the SSH model has proven to predict that are dependent on the values of the intracell and intercell electron hopping probabilities, v and w, respectively [11, 15]. When $v > w$ the SSH model predicted an insulating phase with a well-defined band gap. When $v = w$, the bandgap closed and the model acted as a conductor. Finally, if $v < w$, the model predicted a topological phase with the existence of a bandgap and a pair of edge states within the band gap [11, 15].

Although several mechanical topological insulators have been reported [11], there is no evidence of an experimental implementation of a longitudinal configuration. In this work, we experimentally demonstrate the existence of phase transitions in a longitudinal one-dimensional mechanical topological insulator based on the

SSH model using a system of masses on a slinky acting as sites in the SSH model. We also demonstrate the characteristic properties of topological insulators, i.e., the existence of edge states, exponential decay of amplitude at the edge state, and a winding number different than zero, through a systematic analysis of the geometry of our device. We support our experimental results with a mathematical model based on the classical arrangement of masses in parallel configuration and found that the results match quite well. It is important to notice that this work complements our previous approach to the mechanical topological insulators in an affordable way [11].

2. Experimental methods

2.1. The device

The reported device was composed of a metallic slinky spring of ~ 1.20 m of length, 85 spirals, and 16 metallic masses located at specific positions to emulate the SSH model, see figure 1(a). One of the edges was connected to a mechanical shaker that functioned as the excitation of the device, while the other end was connected to a soft wall to reduce reflections. In our mechanical model, the intra- and inter-cell interactions were mediated by the spring stiffness in those regions. This means that by controlling the spring stiffness between the metallic masses, we were able to manipulate the values of v and w as required by the SSH model [11, 15]. Due to the nature of our device, the control of the position of each metallic mass, and consequently of the stiffness of the spring, was made in terms of the number of spirals in the spring; as expected, the spring stiffness had an inverse relationship with the number of spirals [11], see Supplementary Information (SI) section I.

We fixed the lattice constant to be $\Lambda = 10$ spirals. The distance between the masses was controlled by $d_1 = \Lambda/2 + t$ and $d_2 = \Lambda/2 - t$, the intra- and inter-cell distances, respectively. Here, t is the parameter, in number of spirals, that determined the phase our device displayed. This methodology allowed us to control the stiffness of the spring and, consequently, the interaction strengths. In this sense, $d_1 < d_2$, or $t < 0$, represented the trivial phase, while $d_1 = d_2$ or $t = 0$, and $d_1 > d_2$, or $t > 0$, meant the metallic and topological cases, respectively [15].

2.2. Vibration modes

Our device was designed to prevent transverse modes from appearing by holding the device laterally with 0.1 mm plastic strings, meaning that the masses moved mainly in the longitudinal direction. We found that by measuring the oscillation of a single mass in our device, we could determine the resonant modes of the whole device. This was due to the coupling of the masses through the slinky spring. We selected the first mass A, next to the exciter, see figure 1(a), as the probe mass.

The resonant modes of the device were excited by a square pulse with a duration of 10 ms; a delay of 50 ms was added for convenience in the observation in figure 1(b), panel I. The time width of the pulse was selected to ensure its frequency spectrum was broad enough to contain the frequency region in which we were measuring the resonant modes, see the inset to panel I in figure 1(b). The square pulse generated a mechanical perturbation of amplitude 1 cm that was transmitted to the device by a hard joint between the mechanical shaker and the slinky spring, see panel II in figure 1(b).

Our vibration sensor was composed of a green light emitting diode (LED) powered by a small battery, mounted in the probe mass, and a photodetector located at a fixed distance of 5 cm from the LED. The photodetector measured the intensity of the LED light as a function of its position and time. As our device was restricted to longitudinal oscillations, the change in intensity at the photodetector position changed by about 26% from the rest position to the maximum amplitude of oscillation in the expanded and contracted positions. This change in the intensity was enough to map the oscillations of the probe well beyond the noise level that was measured as 5% of the maximum registered signal, see panel III in figure 1(b). The frequency spectrum from the photodetector signal was measured using a lock-in amplifier. The lock-in amplifier was set to measure a span of 10 Hz centered at 5 Hz, with a resolution of 1024 points. The result was a clear set of peaks located at the resonant modes of the device, see panel IV in figure 1(b). We repeated the procedure for each value of t so the results could be compared, and the different phases of the device observed.

3. Results

It is well known that the phases in the SSH model are topological when the following three conditions are met [11]: 1. Existence of modes in the bandgap; 2. Exponential decay of the amplitude of the edge modes; 3. Winding number 0 and 1 for the trivial and topological phases, respectively. As such, sections 3.1, 3.2, and 3.4 next are dedicated to checking each of these conditions.

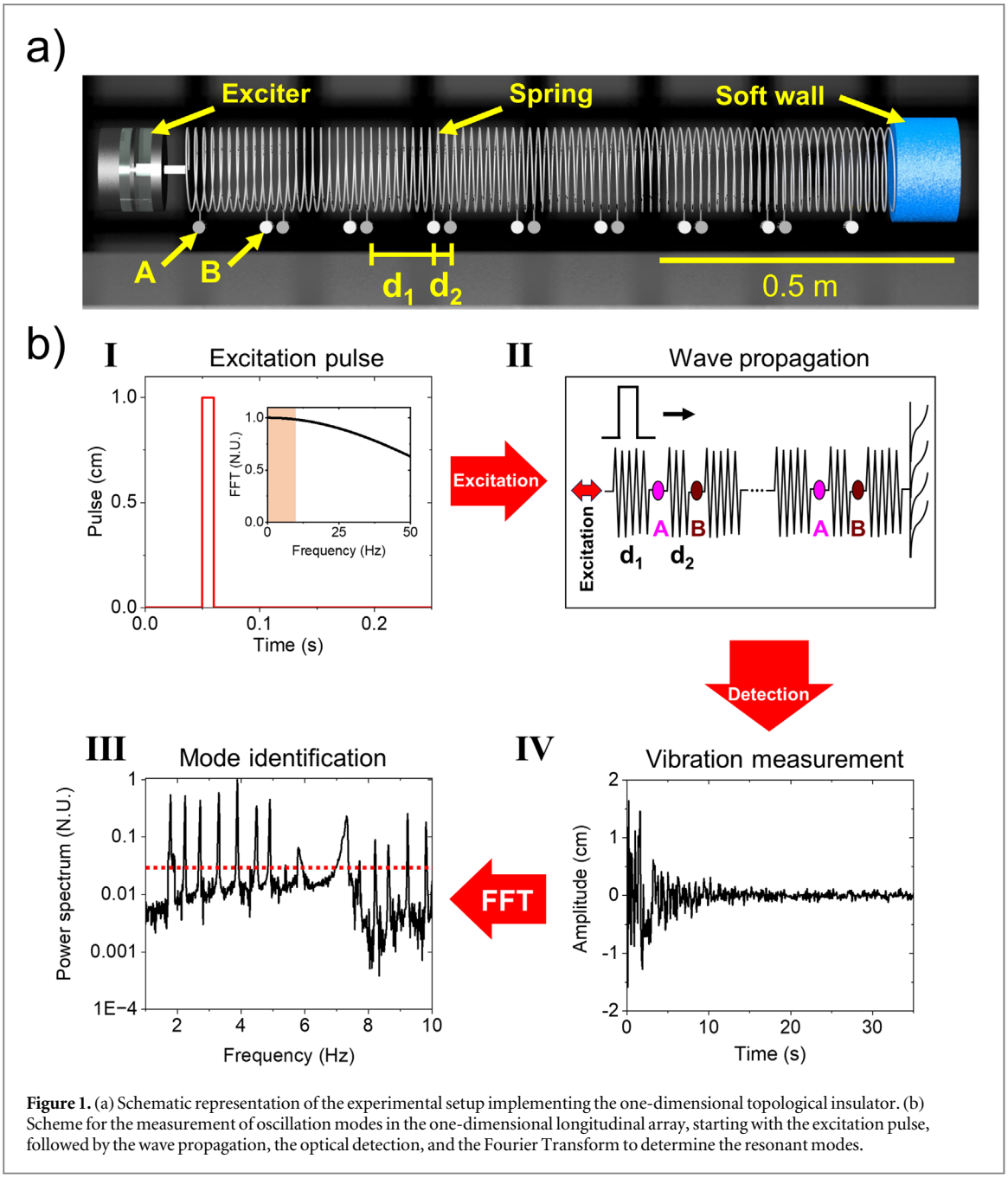

Figure 1. (a) Schematic representation of the experimental setup implementing the one-dimensional topological insulator. (b) Scheme for the measurement of oscillation modes in the one-dimensional longitudinal array, starting with the excitation pulse, followed by the wave propagation, the optical detection, and the Fourier Transform to determine the resonant modes.

3.1. Existence of modes in the bandgap

Each configuration of t, with t an integer, in the range $-4 \leqslant t \leqslant 4$ was tested; we arranged the results in such a way that the different phases were visible. Figure 2 shows a normalized representation of the resonant modes for each of the values of t. As mentioned above, the noise level of our experiments was 5%, see the red dashed line in panel IV of figure 1(b). As such, in figure 2 we limited the signal floor to this value for better observation of the edge modes. Additionally, figure 2 demonstrates that our device presented a bandgap for all the cases in which $t \neq 0$. Moreover, the bandgap was empty for the cases $-4 \leqslant t < 0$ and showed clear edge modes for $0 < t \leqslant 4$, see yellow arrows. This proved that our device exhibited edge modes in the bandgap, so the first condition has been met. Moreover, figure 2 shows the isolation of the edge modes as the value of t increased. It is clear that the edge modes become more defined within a larger bandgap with the increase of t, as expected [11]. We confirmed our experimental results by creating a mathematical model. The mathematical model and comparison with our experimental results are available in sections II and III of the SI. Additionally, we confirmed the robustness of the edge modes with the observation of edge modes even after breaking the symmetry of the first A site, see section IV of the SI. It has been demonstrated that this kind of symmetry breaking does not affect the topological order [16]. A set of previously reported implementations of this preservation of the topological order can be found elsewhere [17, 18].

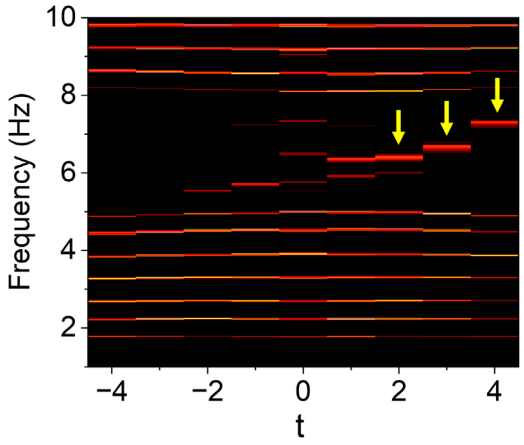

Figure 2. Normalized amplitude of oscillations of experimental frequencies as a function of the parameter t. The color scale has been limited to background noise (0.05).

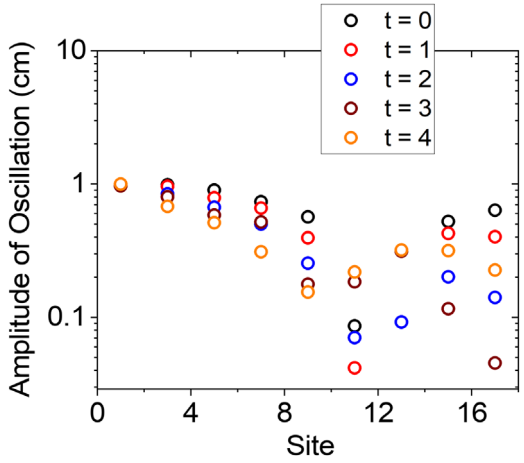

Figure 3. Amplitude of oscillation as a function of the site position for $0 \leqslant t$. Only non-zero amplitudes are shown for better visualization.

3.2. Exponential decay of amplitude

Once we identified the frequencies of the edge modes, we excited the device at those frequencies for values of $0 \leqslant t$ and measured the amplitude of oscillation of each of the masses. As mentioned before, we limited the amplitude of oscillations to remain in the linear regime. This way, we could treat the motion of the masses in our device as a harmonic oscillator, following Hooke's law [19]. It is well-known that the SSH model presents an exponential decay of amplitude in the wave function of the edge states [15]. As such, we expected to see similar behavior in our device, i.e. the amplitude of oscillation to decay exponentially. A visualization of the exponentially decaying energy is available in section V of the SI.

The amplitude of oscillation as a function of the mass position, called site, and t is shown in figure 3. It is clear that the decay of amplitude resembled an exponential function that fit better as t increased. This was an expected result, as larger t meant stronger topological behavior. It is important to note that figure 3 only displays the position of the A masses for a clearer visualization. Additionally, the growth of the amplitude for masses beyond the 10th mass was due to the symmetric behavior of the device, i.e., the edge mode in the opposite site was also weakly excited. Due to this diminishing energy, we only considered masses 1 through 16 for the exponential fits. Also, our device did not show a perfect exponential decay due to imperfections and friction in the device.

The SSH model predicts that only masses in position A will have amplitudes different from zero, meaning all masses in position B must have zero amplitude [11, 15]. In our experimental case, amplitudes of masses in position B were not zero, mainly due to imperfections in the device and friction, as mentioned before, see section V in the SI for further information.

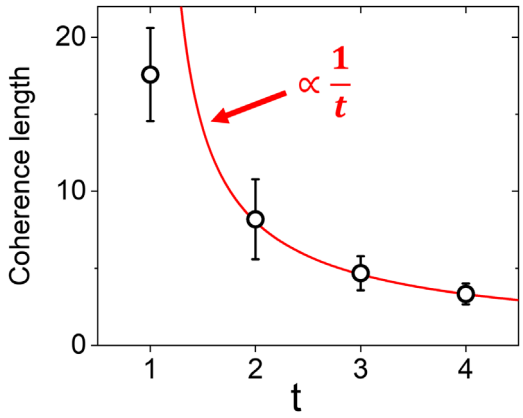

Figure 4. Coherence length as function of t. The black markers represent the experimental values and the red line is a theoretical fit to a function of the form t^{-1}.

Table 1. Winding number calculated with equation (2). The values of k_1 and k_2 are the same as those shown in figure S1.

t	k_1	k_2	ν
−4	8.71 ± 1.40	25.75 ± 2.02	0
−3	9.57 ± 1.61	21.66 ± 5.79	0
−2	10.65 ± 2.04	18.39 ± 3.78	0
−1	11.99 ± 2.51	15.77 ± 3.12	0
0	13.67 ± 2.95	13.97 ± 2.95	Undefined
1	15.77 ± 3.12	11.99 ± 2.51	1
2	18.39 ± 3.78	10.65 ± 2.04	1
3	21.66 ± 5.79	9.57 ± 1.61	1
4	25.74 ± 2.02	8.71 ± 1.40	1

3.3. Winding number

The winding number is a topological invariant in the SSH model and it is a function of k_1, k_2, and t. The winding number (ν) is defined as [15]:

$$\nu = \frac{1}{2\pi i}\int_{-\pi}^{\pi} dk \frac{d}{dk}\log(h(k)) \tag{1}$$

where $h(k) = -k_1/k_2 - \cos(k\Lambda) - i\sin(k\Lambda)$ for our system, see section II in SI. After substituting these values in equation (1), we computed, using Wolfram Mathematica 13 [20]:

$$\nu = \frac{\left(k_1 + k_2 - k_1\sqrt{\frac{(k_1+k_2)^2}{(k_1-k_2)^2\Lambda^2}} + k_2\sqrt{\frac{(k_1+k_2)^2}{(-k_1+k_2)^2\Lambda^2}}\right)\Lambda}{2(k_1+k_2)} - \frac{\arctan\left(\frac{(k_1+k_2)\cot\left(\frac{\Lambda\pi}{2}\right)}{k_1-k_2}\right)}{\pi} \tag{2}$$

Using equation (2), we calculated the winding number as a function of k_1, k_2, and Λ for the different values of t shown in figure 2. The values of ν are shown in table table:1. It is clear that $\nu = 0$ for $t < 0$ and $\nu = 1$ for $0 < t$, as expected [15]. The uncertainty of the winding number has been omitted in table 1 for clarity purposes but was measured to be $\Delta\nu = \pm 0.17$, i.e., small enough to not affect our results. These results confirmed that the topological invariant was confirmed in our experiment.

3.4. Phase transition

In order to complete our discussion about the nature of the reported device, we determined the value of t at which the phase transition happened [11, 21, 22]. This was concluded using the coherence length (CL), defined as the decay constant in the energy in figure 3. The CL must fit to a function of the form t^{-1} [11] after the phase transition, i.e., the critical exponent is -1 [21, 22], reported for the first time in [23]. Figure 4 shows the experimental results (black markers) and theoretical fit (red line) of the CL. It is clear that the CL dependence as t^{-1} happened for $t \geqslant 2$. The fact that the value of the CL does not match the theoretical fit, red line in figure 4, for $t < 2$ is due to the well-known nature of the SSH model [15], i.e., the topological phase transition did not

necessarily occur at the first value beyond the metallic case; confirming one more time the topological nature of our device. Finally, the error bars were calculated as the standard deviation of the values obtained after three experiments. In the case of $1 < t$, the error bars were duplicated in size to make them visible in the current plot settings. As expected, the size of the error bars decreased as t increased due to the stronger topological behavior of the device for large values of t.

4. Conclusions

In summary, we have demonstrated a longitudinal mechanical topological insulator based on a slinky spring. Our results have proven the inherent characteristics of a topological insulator, that is, the existence of states in the bandgap, the exponential decay of the energy, and a winding number of zero for the trivial case and one for the topological case. A theoretical model supported our experimental findings. In addition, we have demonstrated that the edge states are robust against disorder and that the critical exponent is -1 after the phase transition. Finally, our study opens the possibility of studying the nature of topological phases using simple materials available to anyone.

Data availability statement

All data that support the findings of this study are included within the article (and any supplementary files).

ORCID iDs

Juan M Merlo https://orcid.org/0000-0002-3956-0940

References

[1] Hasan M Z and Kane C L 2010 Colloquium: topological insulators *Rev. Mod. Phys.* **82** 3045
[2] Qi X-L and Zhang S-C 2011 Topological insulators and superconductors *Rev. Mod. Phys.* **83** 1057
[3] Jotzu G, Messer M, Desbuquois R, Lebrat M, Uehlinger T, Greif D and Esslinger T 2014 Experimental realization of the topological haldane model with ultracold fermions *Nature* **515** 237
[4] Moore J E 2010 The birth of topological insulators *Nature* **464** 194
[5] Zangeneh-Nejad F, Al'u A and Fleury R 2020 Topological wave insulators: a review *Comptes Rendus. Physique* **21** 467
[6] Zhang X, Xiao M, Cheng Y, Lu M-H and Christensen J 2018 Topological sound *Commun. Phys.* **1** 97
[7] He C, Ni X, Ge H, Sun X-C, Chen Y-B, Lu M-H, Liu X-P and Chen Y-F 2016 Acoustic topological insulator and robust one-way sound transport *Nature Phys.* **12** 1124
[8] Jalali Mehrabad M, Mittal S and Hafezi M 2023 Topological photonics: fundamental concepts, recent developments, and future directions *Phys. Rev.* A **108** 040101
[9] Merlo J M, Wu X, Kempa K and Naughton M J 2021 All-optical logic gates based on anomalous floquet photonic topological insulator structures *J. Opt.* **23** 065001
[10] Zheng S, Duan G and Xia B 2022 Progress in topological mechanics *Applied Sciences* **12** 1987
[11] Thatcher L, Fairfield P, Merlo-Ramrez L and Merlo J M 2022 Experimental observation of topological phase transitions in a mechanical 1d-SSH model *Phys. Scr.* **97** 035702
[12] Su W P, Schrieffer J R and Heeger A J 1979 Solitons in polyacetylene *Phys. Rev. Lett.* **42** 1698
[13] Muhammad, Ogun O and Kennedy J 2023 Inverse design of a topological phononic beam with interface modes *J. Phys. D: Appl. Phys.* **56** 015106
[14] Bleckmann F, Cherpakova Z, Linden S and Alberti A 2017 Spectral imaging of topological edge states in plasmonic waveguide arrays *Phys. Rev.* B **96** 045417
[15] Asbth J K, Oroszlny L and Plyi A 2016 *A Short Course on Topological Insulators , Lecture Notes in Physics* Vol. 919 (Springer International Publishing)
[16] Oliveira L A and Chen W 2024 Robustness of topological order against disorder *Phys. Rev.* B **109** 094202
[17] Jiang J, Guo Z, Ding Y, Sun Y, Li Y, Jiang H and Chen H 2018 Experimental demonstration of the robust edge states in a split-ring-resonator *Opt. Express* **26** 12891
[18] Cáceres-Aravena G, Real B, Guzmán-Silva D, Amo A, Torres L E F F and Vicencio R A 2022 Experimental observation of edge states in ssh-stub photonic lattices *Phys. Rev. Res.* **4** 013185
[19] Choi K, Jiang S and Li Z 2002 Spatial stiffness realization with parallel springs using geometric parameters *IEEE Trans. Robot. Automat.* **18** 274
[20] W. R. Inc. 2024 Mathematica, Version 14.1 , champaign, IL
[21] Chaikin PM L T 1995 *Principles of Condensed Matter Physics* (Cambridge University Press)
[22] Chen W and Schnyder A P 2019 Universality classes of topological phase transitions with higher-order band crossing *New J. Phys.* **21** 073003
[23] Chen A R W, Legner M and Sigrist M 2017 Correlation length, universality classes, and scaling laws associated with topological phase transitions *Phys. Rev.* B **95** 073003